Intelligent Computing
A SCIENCE PARTNER JOURNAL

RESEARCH ARTICLE

Using Exceptional Attributed Subgraph Mining to Explore Interindividual Variability in Odor Pleasantness Processing in the Piriform Cortex and Amygdala

Maëlle Moranges[1,2*], Arnaud Fournel[1], Marc Thévenet[1], Marc Plantevit[2,3], and Moustafa Bensafi[1*]

[1]Lyon Neuroscience Research Center, CNRS UMR5292, INSERM U1028, Université Claude Bernard Lyon 1, Lyon, France. [2]Laboratoire d'InfoRmatique en Image et Systèmes d'information (LIRIS), Université Lyon 1, Lyon, France. [3]EPITA Research Laboratory (LRE), Paris, France.

*Address correspondence to: maelle.moranges@inserm.fr (M.M.); moustafa.bensafi@cnrs.fr (M.B.)

In humans, the amygdala and piriform cortex are 2 important brain structures involved in hedonic odor processing. Although the affective processing of odors in these 2 structures has been extensively studied in the past, the way in which each tested individual contributes to the observed global pattern remains little understood at this stage. The purpose of this study is to examine whether exceptional pattern extraction techniques can improve our understanding of hedonic odor processing in these brain areas while paying particular attention to individual variability. A total of 42 volunteers participated in a functional magnetic resonance imaging (fMRI) study in which they were asked to smell 6 odors and describe their hedonic valence. Classical univariate analyses (statistical parametric mapping) and data mining were performed on the fMRI data. The results from both analyses showed that unpleasant odors preferentially activate the anterior part of the left piriform cortex. Moreover, the data mining approach revealed specific patterns for pleasant and unpleasant odors in the piriform cortex but also in the amygdala. The approach also revealed the contribution of each of the 42 individuals to the observed patterns. Taken together, these results suggest that the data mining approach can be used—with standard fMRI analyses—to provide complementary information regarding spatial location and the contribution of individuals to the observed patterns.

Citation: Moranges M, Fournel A, Thévenet M, Plantevit M, Bensafi M. Using Exceptional Attributed Subgraph Mining to Explore Interindividual Variability in Odor Pleasantness Processing in the Piriform Cortex and Amygdala. *Intell. Comput.* 2024;3:Article 0086. https://doi.org/10.34133/icomputing.0086

Submitted 18 October 2023
Accepted 6 February 2024
Published 1 August 2024

Introduction

The sense of smell is an important sensory function for humans: It allows one not only to detect dangers in the environment but also to feel pleasure [1,2]. Psychophysical and neurobiological studies show that this hedonic processing of odors is omnipresent during the cerebral treatment of an odor: From a neural point of view, the pleasant/unpleasant character of an odor is represented at several levels, in the olfactory epithelium [3], the olfactory bulb [4], the piriform cortex [5,6], the amygdala [7], and the orbitofrontal cortex [8].

Another important aspect of these hedonic processes in relation to odors is that they can vary greatly from one individual to another. While for some people the eugenol molecule is reminiscent of the smell of cloves and can be perceived as rather pleasant, for others it will evoke the rather unpleasant context of the dentist [9]. These interindividual variations in response to smells are little taken into account in olfactory brain imaging studies [10]. Moreover, this variability could explain, at least in part, contradictory results about the role of certain structures in olfactory affective processes from one study to another. Among these structures, 2 areas are particularly studied: the piriform cortex and the amygdala.

Although some studies show that activity within the piriform cortex and amygdala is not associated with valence but rather with the intensity of the olfactory stimulus [11–13], other studies state that the hedonic valence of odors is represented in both structures [7,14]. Still, others suggest that the amygdala encodes neither stimulus intensity nor odor valence, but a combination of both dimensions that reflects the overall emotional salience of the olfactory stimulus [15]. Furthermore, studies that consider valence independently of intensity show that pleasant and unpleasant odors induce a greater neural response in the amygdala [16] and anterior piriform cortex (AntPC) [14] compared to odors described as neutral (without salient emotional valence). Moreover, it appears that this region encompassing the piriform cortex and the amygdala is more activated for unpleasant odors than for pleasant ones [8], with a preponderant involvement of the anterior portion of the piriform cortex. A lateralization of these olfactory hedonic processes in the left part of the AntPC has also been mentioned [5,17]. It should be noted that other studies suggest

that the posterior portion of the cortex is more involved in processing the quality of an odor (e.g., fruity and floral) than the hedonic valence or the perceived intensity of the stimulus [14,18].

In summary, we can understand from this series of brain imaging studies of the sense of smell that the piriform cortex and the amygdala are indeed involved in odor hedonic processes. Nevertheless, the spatial localization of pleasant and unpleasant hedonic representations within this piriform/amygdala network remains to be determined, as does whether interindividual variability in odor hedonic perception can help explain odor pleasantness processing and brain activity in both areas. Although the most commonly used statistical methods (e.g., the general linear model, classification, and multivariate analysis) allow a fine analysis of pleasant and unpleasant hedonic representations of odors, they are most often used in group analyses that combine information from all subjects and take little account of interindividual variability. Interestingly, beyond these conventional approaches, there are other techniques from data science that are still too rarely used in the field of brain imaging that could nevertheless provide complementary information. Among these approaches, we highlight exceptional model mining (EMM).

EMM is used to identify partitions of data where a model fitted to the target variables is significantly different from this same model applied to the entire dataset [19]. An EMM algorithm named C-energetics [20] allows the detection of exceptional subgraphs in an attributed and valued graph: It detects hotspots for different experimental conditions (e.g., pleasant and unpleasant odors) in specific spaces (e.g., piriform cortex and/or amygdala). This approach is freed from smoothing because of modeling in the form of a graph; the graph allows the consideration of not only one voxel but also a voxel and its adjacent voxels. It also overcomes the normalization of the hemodynamic signal per individual by considering the order of activation of experimental trials (e.g., odors) for each individual. Interestingly, once the subgraphs have been generated, it is possible to quantify and study the participation of each individual in the pattern. This allows a more fine-grained analysis of the individual contribution of each participant to activation patterns qualified as invariant.

The main aim of our study is thus to use the EMM approach to describe how interindividual variability in hedonic odor perception can influence olfactory brain activity, particularly within the piriform cortex and amygdala. To this end, our study presents an analysis framework on a dataset comprising 42 volunteers who smelled 6 odors and whose hemodynamic activity in response to these stimuli was recorded using functional magnetic resonance imaging (fMRI). The data were first processed with conventional univariate analyses [e.g., general linear model and region of interest (ROI) analysis in statistical parametric mapping]. In a second step, the data were subjected to EMM in order to provide (a) specific spatial activation patterns in response to the olfactory conditions (e.g., pleasant and unpleasant) and (b) complementary information to the univariate analyses by modeling the contribution of each participant to the activation spatial patterns observed in each ROI (e.g., the piriform cortex and amygdala) and each olfactory condition (e.g., pleasant and unpleasant). Finally, it should be noted that the 42 individuals tested differed in age and gender, enabling us to include the effect of these 2 important variables in olfaction [21–23].

Materials and Methods

Experimental procedure

Participants

The present study includes a dataset of 42 participants divided into 3 subsets. The first dataset (subset 1) is original (never published) and concerns 14 right-handed young adults (6 males and 8 females; mean age 22.86 ± 3.25 years) who smelled 6 odors varying in hedonic quality. The second dataset (subset 2) concerns 15 right-handed young adults (mean age 22.13 ± 4.26 years; 7 males and 8 females) who smelled 6 odors also varying in hedonic quality, but different from those used in subset 1. Note that this second dataset has already been exploited in a previous study [24]. Finally, the third dataset (subset 3) is original and involves 13 elderly right-handed individuals (mean age 63.0 ± 4.08 years; 4 males and 9 females) who smelled the same 6 odors as the volunteers in subset 2. With such an experimental design, it is thus possible to study whether the results observed in elderly versus young adults, or participants who smelled different sets of odors, participate in the same way in the observed patterns. It should of course be noted that the 42 participants that make up this dataset, whatever the subset, performed the experiment under the same experimental conditions (same MRI scanner, same olfactometer, same experimental task, etc.). Only their age or the set of odors differed.

The absence of olfactory deficit was assessed using the European Test of Olfactory Capabilities [25,26], together with a detailed medical history and ear, nose, and throat examination. They received financial compensation for the time spent in the laboratory. The recording procedure was explained in great detail to the subjects, who provided written consent prior to participation. The study was conducted according to the Declaration of Helsinki and was approved by the Lyon Sud-Est ethics committee.

Odorants

All odorants were provided by Sigma-Aldrich. Their names, codes, compound identification (CID) numbers, and concentrations are listed in Table 1 alongside the subset in which they were used.

Note that to ensure isointense perception, odorants were individually diluted in mineral oil (see their respective volume/volume concentrations). Whatever the subset, the odorants were delivered by an air-dilution olfactometer, described in detail by Sezille et al. [27]. Briefly, the device includes a stimulation system, a mixing head coupled to a delivery system enabling diffusion of odorized air in the subject's nose, a respiratory sensor that triggers the olfactometer according to the subject's nasal respiration, and a response box used to collect subjective odor evaluations. The olfactometer, digitized visual instruction generator, recording of respiratory data, and the MRI scanner itself were all linked through one transistor–transistor logic pulse that assured accurate time locking of all experimental components. This was done by recording intranasal sniffing continuously during the experimental session (see the next section).

Experimental protocol

An event-related design was used, comprising the odorants (10 trials per olfactory stimulus, 20-s interstimulus interval, and

Table 1. Odorants used in the study

Subset	Odorant	Odorant code	CID	Volume/ volume concentration
1	Heptanal	HEP	8130	0.15%
	1-Decanol	DEC	8174	100%
	Acetophenone	ACE	7410	4.8%
	Eugenol	EUG	3314	59%
	Methyl anthranilate	MAN	8635	65.7%
	3-Hexanol	3HEX	12178	0.17%
2 and 3	Propanol	PRO	1031	1.5%
	Isoamyl acetate	ISO	31276	0.6%
	Benzaldehyde	BEN	240	75%
	Citronellal	CAL	7794	15%
	Citronellol	COL	8842	22.5%
	Trans-2-hexenyl acetate	THA	17243	1.5%

5-s stimulus duration) and a non-odorized clean air condition, all trials distributed randomly across 5 fMRI scans (sessions). Each trial began with a 2-s visual primer ("Breathe naturally") followed 5 s later by a 5-s hedonic task instruction ("Rate the hedonic valence"). Practically, participants were instructed to breathe naturally, and after the presentation of each olfactory stimulus (for 5 s), they were asked to evaluate odor hedonic valence using a response box with 5 buttons positioned under the 5 fingers of the dominant hand. The participants had 5 options: very unpleasant smell, unpleasant smell, neutral smell, pleasant smell, very pleasant smell. The positioning of the options under the fingers was counterbalanced from one participant to another (i.e., the thumb corresponded to very pleasant for half of the subjects and very unpleasant for the other half). Odorants were diffused synchronously with the subject's nasal respiration: A 5-s stimulus duration was chosen because the odor was released during exhalation and had to be maintained during at least the whole duration of the subsequent inhalation (approximately 2 s). The recorded signals were as follows: respiratory signal, odor valve opening, and time repetition (TR) signal from the fMRI scanner, enabling event-related statistical analysis. Subject's respiratory signal was acquired using an airflow sensor that was integrated on an amplifier interface. A microbridge mass airflow (AWM2100V, Honeywell, MN, USA) allowed acquisition of both inhalation and exhalation phases. The airflow sensor was connected to a nasal cannula (Cardinal Health, OH, USA; 2.8-mm-inner-diameter tube) positioned in both nostrils. Sniffing was digitally recorded at 100 Hz and stored in a computer. Sniffs were preprocessed by removing baseline offsets and aligned in time by setting the point where the sniff entered the inspiratory phase as time zero. Inspired volume was calculated for the first sniff of every trial and was used as a covariate in the fMRI contrast estimation.

Note that at the end of the fMRI sessions, participants were asked to rate the odorants in terms of pleasantness, intensity, familiarity, edibility, warmth, coolness, irritation, and pain, using a visual rating scale ranging from −2 (very unpleasant) to 2 (very pleasant), or from 0 (not at all intense, familiar, edible, warm, cool, irritating, or painful/pungent) to 4 (very intense, familiar, edible, warm, cool, irritating, or painful/pungent).

fMRI parameters

The experiment, which lasted approximately 60 min (from subject's arrival to departure), was performed on a 1.5-T MR scanner (Siemens Magnetom). The fMRI data were collected in 142 volumes per session (interleaved, anterior commissure-posterior commissure acquisition) with a 29 axial-slice 2-dimensional (2D) echo planar imaging (EPI) sequence (matrix: 64 × 64; time of repetition (TR): 2,500 ms; time to echo (TE): 50 ms; flip angle (FA): 90°; voxel size: 3.43 × 3.43 × 3.4 mm; field of view (FOV): 220). In the 9 min immediately following the fMRI session, a high-resolution T1-weighted brain image (3D multiplanar reconstruction (MPR) sequence: TR = 1,970 msTE = 3.93 ms) was acquired.

Data analysis

Preprocessing of perceptual data

Hedonic ratings during the fMRI sessions were averaged for the 10 trials of the same odorant. Then, a discretization was performed in these values for each volunteer independently with a *K*-means clustering algorithm [28]. For a given volunteer, *K*-means divides the subjective ratings (of the 6 odors) into *K* clusters so that the intracluster distance of the scores is minimized and the intercluster distance is maximized. This technique is independent of participants' scoring strategies because the discretization is applied at the individual level and yields the 3 categories of odors experienced as differently as possible in terms of pleasantness [29]. We chose $K = 3$ so that the cluster with the highest values corresponds to pleasant odors, the cluster with the lowest values corresponds to unpleasant odors, and the middle cluster corresponds to neutral odors. In total, the proportions of responses between the 3 categories across all participants were fairly well balanced (unpleasant: 35.32%; neutral: 36.90%; pleasant: 27.78%).

fMRI preprocessing and first-level analysis

Functional MRI images were preprocessed using fMRIPrep [30] including the following standard steps: (a) realignment of the voxels to correct the movements, (b) correction for temporal acquisitions, (c) coregistration of functional and structural images, (d) segmentation of the T1 image, (e) application of the deformation so that the images of the individual fit into the template image, and (f) estimation of regressors of no interest. At this stage of preprocessing, 2 datasets have been constructed. For the univariate analyses (see the next section), voxels were smoothed using a $5 \times 5 \times 5$ mm^3 full width at half maximum (FWHM) Gaussian kernel to limit potential noise. For the data mining analyses (see the "Data mining analysis" section), the data were left in their raw state because the algorithm searches for a set of adjacent voxels having an exceptional and similar behavior. Smoothing the data would artificially create similar behavior between adjacent voxels, and the algorithm would thus return biased patterns. The algorithm maximizes the

size of the pattern so that a noisy voxel will not stand out in the results. Then, these 2 datasets (smoothed and unsmoothed) were subjected to first-level analyses. Here, to obtain the estimated activity of each voxel and for each odor, voxel responses were modeled using a design matrix: (a) built with a canonical hemodynamic response function and regressors of interest corresponding to 3 conditions of pleasantness (pleasant, neutral, unpleasant) for the univariate analysis (note that for this analysis, a fourth condition combining all odors was also performed to build a functional group image in response to all olfactory stimuli), and (b) built with a canonical hemodynamic response function and regressors of interest corresponding to the 6 odors (subset 1: HEP, MAN, 3HEX, DEC, ACE, EUG; subsets 2 and 3: PRO, ISO, CAL, BEN, COL, THA) for the data mining analysis. The following signals were added to the model as nuisance regressors: 6 first aCompCor components [31], 6 motion parameters, frame displacements, nasal respiration (downsampled to fMRI frequency), and a cosine basis set acting as a high-pass filter (with a 128-s cutoff). Finally, for each participant, the final contrasts consisted in comparing each of the 3 conditions of pleasantness (for the univariate analyses) or the 6 odors (for the data mining analysis).

Univariate analysis

The univariate analysis is not innovative in the present study. As its purpose is to present the data using standard approaches that are widely documented in the literature, we will present it in a summary manner and refer the reader to the already existing documentation (see [32]). Here, the approach is based on a group analysis on the statistical parametric mapping software, which is obtained using single-sample t tests ($P < 0.001$, uncorrected). The coordinates of the MNI (Montreal Neurological Institute) space are used to present all activations. Then, a specific analysis in the piriform cortex and amygdala, our different ROIs, was performed. Note that for the piriform cortex ROI, we distinguished its anterior part from its posterior part since previous studies suggest a different functional role in each of these subregions. The amygdala ROI (in both the left and right hemispheres) was obtained from the automated anatomical atlas template [33–35]. Anterior and posterior piriform left/right ROI activity was extracted using hand-drawn ROIs. These ROIs were drawn with the MRIcron application using 60 participants who had participated in previous studies [36]. An illustration of the 3 ROIs is available in Fig. S1. Resulting mean images were thresholded to obtain a binary mask: At least 30% of participants had to have a voxel in their ROI to keep it in the binary mask. We then performed analyses of variance on the average activity extracted in each ROI to examine whether the activation within each ROI differs between hemispheres and olfactory conditions (pleasant, neutral, and unpleasant stimuli). We also looked for an interaction between these 2 factors.

Data mining analysis

The data mining analysis is composed of 6 steps. The first one is common with univariate analysis and concerns preprocessing as was presented previously ("Preprocessing of perceptual data" and "fMRI preprocessing and first-level analysis" sections). In this section, we introduce the remaining steps. The second step is to model the data in the form of an attributed graph, and we continue with the generation of patterns using data mining algorithms. Next, we present the validation of these results by bootstrap, and finally, we calculate the participation of each individual in the observed patterns and visualize the results. This workflow is illustrated in Fig. 1.

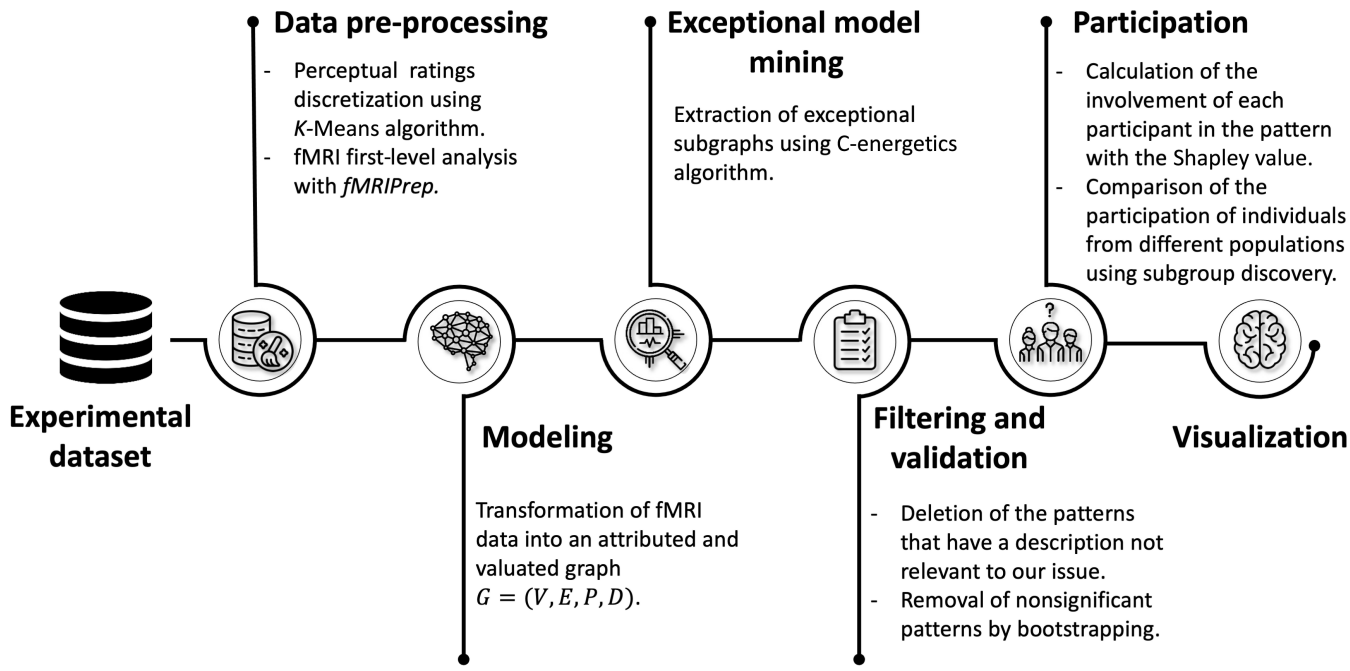

Fig. 1. Steps of the workflow. (1) The raw fMRI data from the experiment are preprocessed, and the subjective scores are discretized into 3 categories for each individual. (2) Once the data are cleaned, they are transformed into an attributed and valued graph. (3) This graph is given as input to the EMM algorithm in order to extract voxel subsets describing the different perceptual dimensions. (4) Then, a statistical validation of the generated patterns is performed: the pattern is validated if its quality measure (called WRAcc) is outside the confidence interval of the distribution of a bootstrap of 10,000 random draws. (5) Finally, the participation of each individual in the pattern is calculated, and (6) the results can be visualized.

Note that in this analysis, our interest is not in the absolute value of the voxels for each odor but rather in the relative order of the value of the voxels for each odor (compared to all other odors) within each subject. In this way, there is no need to normalize the signals of the participants to compare them.

a. Modeling

The aim of this step is to transform the fMRI data into an attributed graph. These data are composed of one fMRI image by participant (or individual) and by odor and a subjective hedonic rating for a given odor. Let $A = \{$'*pleasant*','*neutral*','*unpleasant*'$\}$ be the set of hedonic categories studied. Let $\pi_i[o]$ such that $\pi_i[o] \in A$ be the category used by the individual i to describe the pleasantness of the odor o $\in O$. O is the set of odorants such that $O = \{$'*HEP*', '*MAN*','*3HEX*', '*DEC*', '*ACE*', '*EUG*', '*PRO*', '*ISO*', '*CAL*', '*BEN*', '*COL*', '*THA*'$\}$.

An fMRI image is composed of several voxels, and each voxel contains a hemodynamic activation value β. These voxels are considered here as the vertices V of a graph $G = (V, E, P, D)$ whose edges E connect the adjacent voxels in the fMRI image. The vertex v representing a voxel at position (x, y, z) is thus connected to the voxels at the following positions: $(x-1, y, z)$, $(x+1, y, z)$, $(x, y-1, z)$, $(x, y+1, z)$, $(x, y, z-1)$, and $(x, y, z+1)$, if these neighboring voxels are included in the ROI studied.

The set $P = \{(\alpha, \alpha') \mid \alpha \in A, \alpha' \in A \text{ and } \alpha \neq \alpha'\}$ contains all combinations of 2 non-identical categories. As an example, the pair ('*pleasant*','*neutral*') $\in P$ aims at depicting the number of cases where odors perceived as neutral have a stronger hemodynamic response than pleasant-perceived odors. To this end, we need to count for each vertex (i.e., voxel) the number of times each possible pair appears.

We denote by $X(v, i, o)$ the level of β activity measured in the vertex v for an individual $i \in [1, n]$ while smelling an odorant o.

We introduce as vertex attributes the pairs of categories from P. Therefore, for each vertex v, each pair $p = (\alpha, \alpha')$ is associated with a unique value d because of the function $d(p, v)$:

$$d(p,v) = \sum_{i=1}^{n} \frac{\left|\left\{(o_1,o_2) \in O^2 \middle| \pi_i[o_1] = \alpha, \pi_i[o_2] = \alpha', X(v,i,o_1) < X(v,i,o_2)\right\}\right|}{\left|\{o \in O \mid \pi_i[o] = \alpha\}\right| . \left|\{o \in O \mid \pi_i[o] = \alpha'\}\right|}, \quad \text{with } p = (\alpha, \alpha') \tag{1}$$

The value d for a vertex (i.e., a voxel) v and a pair p is the sum of the average occurrence of the pair for each individual. The average occurrence of a pair for an individual is between 0 and 1; the value d for n individuals is therefore between 0 and n. The sum of the value d for a pair and its opposite pair are equal to n: $d((\alpha, \alpha'), v) + d((\alpha', \alpha), v) = n$.

As an example, Fig. 2A presents 6 connected vertices of the graph.

A

$v_1 = (33, 39, 17)$

Pairs	Values
(*pleasant*, *unpleasant*)	18.67
(*unpleasant*, *pleasant*)	23.33
(*pleasant*, *neutral*)	20.25
(*neutral*, *pleasant*)	21.75
(*neutral*, *unpleasant*)	24.17
(*unpleasant*, *neutral*)	17.83

$v_2 = (34, 39, 17)$

Pairs	Values
(*pleasant*, *unpleasant*)	23
(*unpleasant*, *pleasant*)	19
(*pleasant*, *neutral*)	20.08
(*neutral*, *pleasant*)	21.92
(*neutral*, *unpleasant*)	17.25
(*unpleasant*, *neutral*)	24.75

$v_3 = (35, 39, 17)$

Pairs	Values
(*pleasant*, *unpleasant*)	20.58
(*unpleasant*, *pleasant*)	21.42
(*pleasant*, *neutral*)	22.75
(*neutral*, *pleasant*)	19.25
(*neutral*, *unpleasant*)	21.58
(*unpleasant*, *neutral*)	20.42

$v_4 = (33, 40, 17)$

Pairs	Values
(*pleasant*, *unpleasant*)	16.42
(*unpleasant*, *pleasant*)	25.58
(*pleasant*, *neutral*)	18.75
(*neutral*, *pleasant*)	23.25
(*neutral*, *unpleasant*)	21.42
(*unpleasant*, *neutral*)	20.58

$v_5 = (34, 40, 17)$

Pairs	Values
(*pleasant*, *unpleasant*)	18.42
(*unpleasant*, *pleasant*)	23.58
(*pleasant*, *neutral*)	19
(*neutral*, *pleasant*)	23
(*neutral*, *unpleasant*)	19.58
(*unpleasant*, *neutral*)	22.42

$v_6 = (35, 40, 17)$

Pairs	Values
(*pleasant*, *unpleasant*)	22.42
(*unpleasant*, *pleasant*)	19.58
(*pleasant*, *neutral*)	22.75
(*neutral*, *pleasant*)	19.25
(*neutral*, *unpleasant*)	21.17
(*unpleasant*, *neutral*)	20.83

B

Example of dataset

Odorants pleasantness for individuals 1 and 2:

		Odorants					
		HEP	*DEC*	*ACE*	*EUG*	*MAN*	*3HEX*
Individuals	1	*pleasant*	*pleasant*	*unpleasant*	*unpleasant*	*pleasant*	*neutral*
	2	*neutral*	*neutral*	*pleasant*	*unpleasant*	*unpleasant*	*pleasant*

Hemodynamic order of odors for individuals 1 and 2 and voxel v:

X(v, 1,3*HEX*) <X(v, 1, *HEP*) < X(v, 1, *ACE*) < X(v, 1, *DEC*) < X(v, 1, *MAN*) < X(v, 1, *EUG*)
X(v, 2, *ACE*) < X(v, 2,3*HEX*) < X(v, 2, *EUG*) < X(v, 2, *DEC*) < X(v, 2, *HEP*) < X(v, 2, *MAN*)

with in green the odorants o such as $\pi_i[o] =$ '*pleasant*', in orange o such as $\pi_i[o] =$ '*neutral*' and in red o such as $\pi_i[o] =$ '*unpleasant*'.

Attributes of the voxel v in the graph G

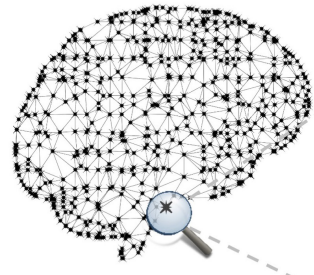

v

Pairs	Values
(*neutral*, *unpleasant*)	2/2+2/4=1.5
(*unpleasant*, *neutral*)	0/2+2/4=0.5
(*neutral*, *pleasant*)	3/3+0/4=1
(*pleasant*, *neutral*)	0/3+4/4=1
(*pleasant*, *unpleasant*)	4/6+4/4=1.66
(*unpleasant*, *pleasant*)	2/6+0/4=0.33

Fig. 2. Graph modeling. (A) Example of distribution of pair value in a subgraph. (B) Calculation of attribute values for a voxel with 2 individuals.

To understand the calculation of D values better, Fig. 2B provides an example using a toy dataset of 2 individuals $I = \{1, 2\}$ and a voxel v. The details of the calculations for the associated value to the pair $(\alpha, \alpha') = (\text{'}neutral\text{'}, \text{'}unpleasant\text{'})$ are presented below.

First, we count the number of odors for '*neutral*' and '*unpleasant*':

For the individual $i = 1$:

$$|\pi_1[o] = \alpha| = \left|\{'3HEX'\}\right| = 1 \tag{2}$$

$$|\pi_1[o] = \alpha'| = \left|\{'ACE', 'EUG'\}\right| = 2 \tag{3}$$

For the individual $i = 2$:

$$|\pi_2[o] = \alpha| = \left|\{'HEP', 'DEC\}\right| = 2 \tag{4}$$

$$|\pi_2[o] = \alpha'| = \left|\{'EUG', 'MAN'\}\right| = 2 \tag{5}$$

Now, we list the pairs (o_1, o_2) such that $\pi_i[o_1] =$ '*neutral*', $\pi_i[o_2] =$ '*unpleasant*', and $X(v, i, o_1) < X(v, i, o_2)$:

For the individual $i = 1$:

$$\left|(o_1, o_2) \mid \pi_1[o_1] = \alpha, \pi_1[o_2] = \alpha', X(v, 1, o_1) < X(v, 1, o_2)\right| = \left|('3HEX', 'ACE'), ('3HEX', 'EUG')\right| = 2 \tag{6}$$

For the individual $i = 2$:

$$\left|(o_1, o_2) \mid \pi_2[o_1] = \alpha, \pi_2[o_2] = \alpha', X(v, 2, o_1) < X(v, 2, o_2)\right| = \left|('DEC', 'MAN'), ('HEP', 'MAN')\right| = 2 \tag{7}$$

The value d associated to the pair $(\alpha, \alpha') = (\text{'}neutral\text{'}, \text{'}unpleasant\text{'})$ is therefore:

$$d((\alpha, \alpha'), v) = \frac{\left|(o_1, o_2) \mid \pi_1[o_1] = \alpha, \pi_1[o_2] = \alpha', X(v, 1, o_1) < X(v, 1, o_2)\right|}{|\pi_1[o] = \alpha|.|\pi_1[o] = \alpha'|} + \frac{\left|(o_1, o_2) \mid \pi_2[o_1] = \alpha, \pi_2[o_2] = \alpha', X(v, 2, o_1) < X(v, 2, o_2)\right|}{|\pi_2[o] = \alpha|.|\pi_2[o] = \alpha'|} \tag{8}$$

$$d((\alpha, \alpha'), v) = \frac{2}{1 \times 2} + \frac{2}{2 \times 2} = 1.5 \tag{9}$$

b. Subgroup discovery: Exceptional attributed subgraph mining

Here, we aim to extract exceptional subgraphs using the C-energetics algorithm. We are looking for sets of connected voxels attributed by pairs whose associated value is exceptionally high compared to the rest of the graph. A high value associated with a pair means that this pair is frequent for many individuals. For example, in Fig. 2A, vertices v_1, v_4, and v_5 have high pairs ('*neutral*','*pleasant*') and ('*unpleasant*','*pleasant*') compared to the rest of the graph. To find these exceptional subgraphs, we use the C-energetics algorithm [20].

This algorithm takes as input a graph with a set of vertices V, a set of edges E, pairs C, and values D. From this graph, it returns patterns each described by a set of vertices $K \subseteq V$, a set of pairs $L \subseteq C$ that maximize a quality measure called weighted relative accuracy (WRAcc) [37]. The measure $WRAcc(L, K)$ quantifies the relevance of the pattern.

We denote by $G[K]$ the subgraph induced by K. We denote by $sum(X, Y)$ the sum of the values associated with the set of pairs X and the set of voxels Y:

$$sum(X, Y) = \sum_{v \in Y} \sum_{p \in X} d(p, v) \tag{10}$$

To evaluate the exceptionality of the values of the pairs L in the subgraph $G[K]$ compared to the rest of the graph, we use the gain function:

$$gain(L, K) = \frac{sum(L, K)}{sum(P, K)} - \frac{sum(L, V)}{sum(P, V)} \tag{11}$$

The gain is equal to the frequency of exceptional pairs reported in the pattern minus the expected value, i.e., the frequency of these exceptional pairs throughout the graph.

For a pair to be included in the pattern, its gain for each voxel in the pattern must be positive. The *valid* function is used to check this condition:

$$valid(L, K) = \wedge_{v \in K} \wedge_{p \in L} gain(p, v) > 0 \tag{12}$$

A pattern is valid if the gain is positive for all the vertices of the pattern $v \in k$ and all the exceptional pairs of the pattern $p \in L$.

The quality of the found pattern can be measured by the weighted relative accuracy function:

$$WRAcc(L, K) = \begin{cases} \frac{sum(K)}{sum(V)} \times gain(L, K) \text{ if } valid(L, K) \\ 0 \text{ otherwise} \end{cases} \tag{13}$$

The WRAcc is zero if the pattern is invalid; otherwise, it is equal to the support of the subgraph multiplied by the gain of the pattern. A positive gain means that the observed values for the pair L in the pattern are higher in the K voxels than expected. The presence of the support allows us to maximize the number of vertices in the pattern.

From a graph $G = (V, E, P, D)$ and 2 thresholds σ and δ, C-energetics returns patterns each as an exceptional subgraph (L, K) such that 1. $|K| \geq \sigma$, 2.$G[K]$ is connected, and 3.$WRAcc(L, K) \geq \delta$.

It is important to note that this algorithm uses a closure operator to avoid redundant patterns.

c. Filtering and validation of patterns

After having applied exceptional attributed subgraph mining to our data, we now need to focus on the patterns that are of interest and/or delete those which appear nonsignificant following bootstrapping. To this end, we first filter the patterns in order to keep only those which interest us in this study. Among

all the generated patterns, we are interested in 2 patterns: (a) the pleasant patterns that have the description "{('*unpleasant*', '*pleasant*'), ('*neutral*', '*pleasant*')}", i.e., pleasant stronger than neutral and unpleasant, and (b) the unpleasant patterns with the description "{('*pleasant*', '*unpleasant*'), ('*neutral*', '*unpleasant*')}", i.e., unpleasant stronger than the 2 other classes. Second, in order to be sure that these patterns of interest are not generated by chance, we apply a validation step. For each pattern, we check that we cannot find a subgraph with a similar WRAcc by randomly drawing nodes in the graph. We calculate the distribution of the WRAcc of 10,000 connected subgraphs of the same size as the subgraph of the pattern for the same exceptional characteristics. If the WRAcc of the pattern is above the confidence interval (with $\alpha = 0.025$) of this distribution, then the pattern is validated; otherwise, it is rejected from our results.

d. Participation of individuals in the patterns

The main aim of our study was to incorporate interindividual variability into the analysis by attempting to assess how each individual contributes to the generated pattern. To do so, we calculated the involvement of each participant in the pattern using the Shapley value and also compared the involvement of individuals from different populations (depending on the odor sets used and/or depending on age) using statistical tests. In this way, we can know if a pattern concerns everyone or only a given population.

Here, in order to know if an individual i participates in the pattern, we took inspiration from game theory with the Shapley value [38]. This measure was initially used to distribute a payoff fairly within a coalition. Here, we used it to distribute the *gain* of the pattern between individuals in order to quantify participation.

We are interested here in the variation (increase or decrease) of gain that the coalition can obtain with the presence of individual i. Shapley value corresponds to the average marginal value of this variation for all possible coalitions with individual i.

The Shapley value for an individual i is denoted $\varphi_i(v)$ and is defined by:

$$\varphi_i(v) = \sum_{Z \subseteq N, i \in Z} \frac{(n - |Z|)!(|Z| - 1)!}{n!} \times (v(Z) - v(Z \setminus i)), \tag{14}$$

where $|Z|$ is the number of individuals in the coalition Z, n is the total number of individuals, and $v(Z)$ is a characteristic function that gives the gain of the coalition Z. The calculation of this value is illustrated in Fig. 3 in an example with 3 individuals.

In our study, the function v is the *gain*(L, K) in the coalition-wide graph only. This graph has the same vertices K and characteristics S, and the value d' associated with a pair p and a vertex v for a coalition Z is given by the function $d'(p, v, Z)$:

$$d'(p, v, Z) = \sum_{Z \subseteq N, i \in Z} \frac{\left|\left\{(o_1, o_2) \in O^2 \middle| \pi_i[o_1] = \alpha, \pi_i[o_2] = \alpha', X(v, i, o_1) < X(v, i, o_2)\right\}\right|}{\left|\{o \in O \mid \pi_i[o] = \alpha\}\right| . \left|\{o \in O \mid \pi_i[o] = \alpha'\}\right|}, \quad \text{with } p = (\alpha, \alpha') \tag{15}$$

The value d' for a vertex (i.e., a voxel) v and a pair p is the sum of the average occurrence of the pair for each individual of coalition Z.

There are $2^{42} - 1$ non-empty coalitions, so calculating the Shapley value is not possible. We therefore approximate this value in polynomial time based on sampling theory with the algorithm ApproShapley [39]. The estimate of the Shapley value is the average of the marginal contributions on a sample of 15,000 random coalitions.

Once the participation of each individual is calculated for a pattern, we can then compare the participation according to other parameters such as age and gender using subgroup discovery algorithm. Our aim is to examine whether specific patterns are more prominently represented by young men, elderly men, young women, or elderly women. To achieve this, all patterns in which an individual participates are represented in the form of itemsets that are labeled according to their age (junior/senior) and sex (male/female), as illustrated in Table 2. Using the MCTSExtent algorithm [40], we extract exceptionally present patterns for each of the 4 classes (Female-Junior, Male-Junior, Female-Senior, Male-Senior).

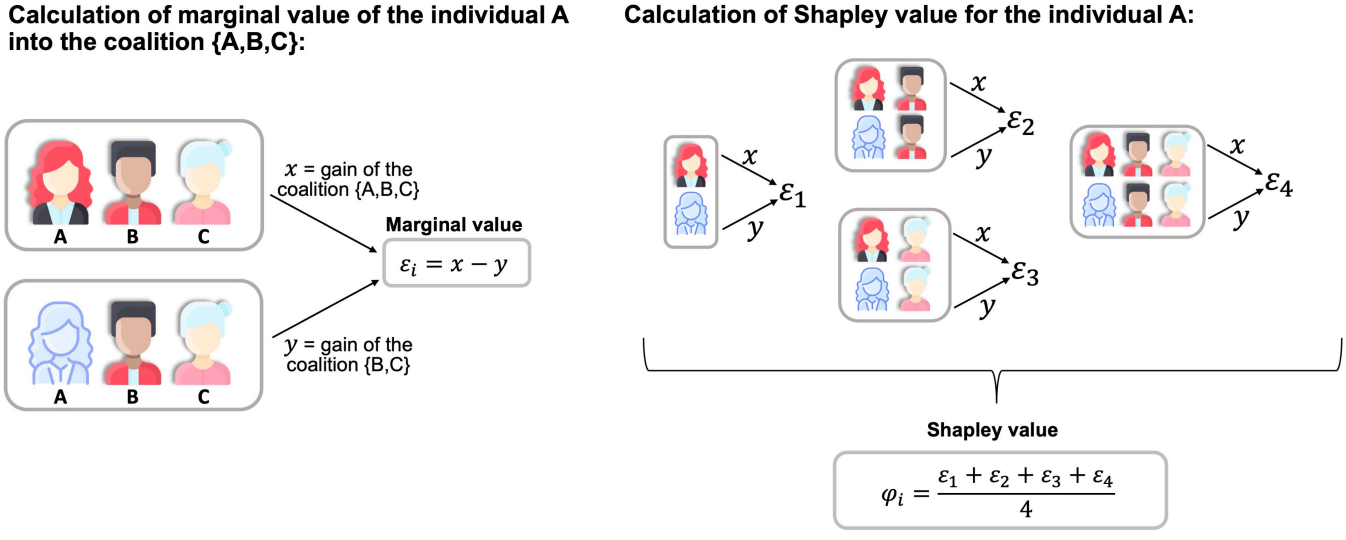

Fig. 3. Calculation of Shapley value for an individual A in a dataset with 3 individuals.

Results

Univariate analysis

Figure 4A depicts the functional group image of all 42 participants smelling in all odorant conditions. This analysis shows both piriform and amygdala activity (for completeness, whole brain activation results are available in Fig. S2 and Table S2). When focusing on each of these areas, for the anterior portion of the piriform cortex, whereas a trend was observed for a valence effect (F[1.84582,75.67787] = 2.86457, P = 0.06737) (Fig. 4B), the hemisphere effect was significant (F[1,41] = 13.09049, P = 0.00081), reflecting a stronger activity in the right hemisphere than in the left (Fig. 4C and D). Interestingly, the hemisphere–valence interaction was significant (F[1.54964,63.53511] = 6.95765, P = 0.00393), reflecting increased hemodynamic activity for unpleasant odors (m = 28.37, IC = [21.37,35.37]) versus neutral odors (m = 11.31, IC = [3.73,18.89]; t (41) = −3.397, P = 0.0015) and pleasant odors (m = 18.95, IC = [9.86,28.04]; t (41) = 2.054, P = 0.0464), specifically in the left hemisphere. The remaining comparisons both in the left and in the right hemisphere did not reach significance (P > 0.05 in all cases).

For the posterior portion of the piriform cortex, whereas the valence effect was not significant (F[1.42119,58.26893] = 0.88564, P = 0.38565), we observed a significant hemisphere effect (F[1,41] = 5.76482, P = 0.02097), reflecting—as for the anterior piriform—a stronger activity in the right than the left hemisphere (Fig. 4E and F). Although the hemisphere–valence interaction was significant (F[1.54616,63.39256] = 3.96834, P = 0.03339), mean comparisons reached significance neither in the left nor in the right hemisphere (P > 0.05 in all cases).

Finally, for the amygdala, no valence (F[1.17687,48.25180] = 1.96652, P = 0.16559) (Fig. 4G) or hemisphere effects (F[1,41] = 2.51956, P = 0.12013) were observed. Note that the hemisphere–valence interaction was also not significant (F[1.21168,49.67871] = 1.10181, P = 0.31189).

Table 2. Format of data used to study the participation of individuals using subgroup discovery

Individual	Itemset of patterns	Class
1	{ #1AntPC, #2AntPC, #3AntPC, #1PostPC, #3PostPC, #4PostPC, #1Amyg, #2Amyg, #3Amyg, #4Amyg, #6Amyg }	Male-Junior
...	...	...
42	{ #2AntPC, #3AntPC, #1PostPC, #2PostPC, #3PostPC, #5PostPC, #1Amyg, #2Amyg, #3Amyg, #4Amyg }	Female-Junior

Data mining analysis

Table 3 lists all patterns extracted by the C-energetics algorithm (WRAcc > 0.0005; validated by bootstrapping; see also Figs. S3 to S5). The patterns are organized by ROI (anterior and posterior parts of the piriform cortex, amygdala) and

Table 3. Patterns extracted by the C-energetics algorithm. The table highlights the ROI on which the search was conducted (column 1), the pattern's rank (column 2), its abbreviated name (column 3), its hedonic category (column 4), the WRAcc value, indicating the pattern's measurement quality (column 5), the number of voxels in the pattern (column 6), the percentage of individuals participating in the pattern (column 7), the coordinates of the pattern's center of mass (column 8), and the hemisphere where the pattern is located (column 9).

ROI	Rank	Pattern	Hedonic category	WRAcc	|Voxels|	Participation (%)	Coordinates of mass center (X,Y,Z)	Lateralization
Anterior piriform cortex (63 voxels)	1	#1AntPC	Unpleasant	0.01151	9	52.38	(−31.18,11.90,−17.30)	Left
	2	#2AntPC	Pleasant	0.00712	7	45.24	(37.58,11.90,−17.30)	Right
	3	#3AntPC	Pleasant	0.00519	5	61.90	(23.83,11.90,−20.70)	Right
Posterior piriform cortex (125 voxels)	1	#1PostPC	Unpleasant	0.00626	12	59.52	(−20.86,1.58,−13.90)	Left
	2	#2PostPC	Pleasant	0.00497	9	52.38	(−31.18,5.02,−17.30)	Left
	3	#3PostPC	Unpleasant	0.00329	6	66.67	(−27.74,5.02,−24.10)	Left
	4	#4PostPC	Pleasant	0.00287	4	50	(27.30,1.58,−10.50)	Right
	5	#5PostPC	Pleasant	0.00221	3	52.38	(16.95,5.02,−20.70)	Right
Amygdala (179 voxels)	1	#1Amyg	Unpleasant	0.002499	13	54.76	(−20.86,−1.86,−13.90)	Left
	2	#2Amyg	Pleasant	0.002469	12	59.52	(−27.74,−5.29,−17.30)	Left
	3	#3Amyg	Pleasant	0.001826	8	50	(27.27,−1.86,−24.10)	Right
	4	#4Amyg	Pleasant	0.001397	7	47.62	(23.83,−1.86,−10.50)	Right
	5	#5Amyg	Unpleasant	0.001087	5	52.38	(30.71,−5.29,−17.30)	Right
	6	#6Amyg	Pleasant	0.000710	3	42.86	(−24.30,1.58,−27.50)	Left

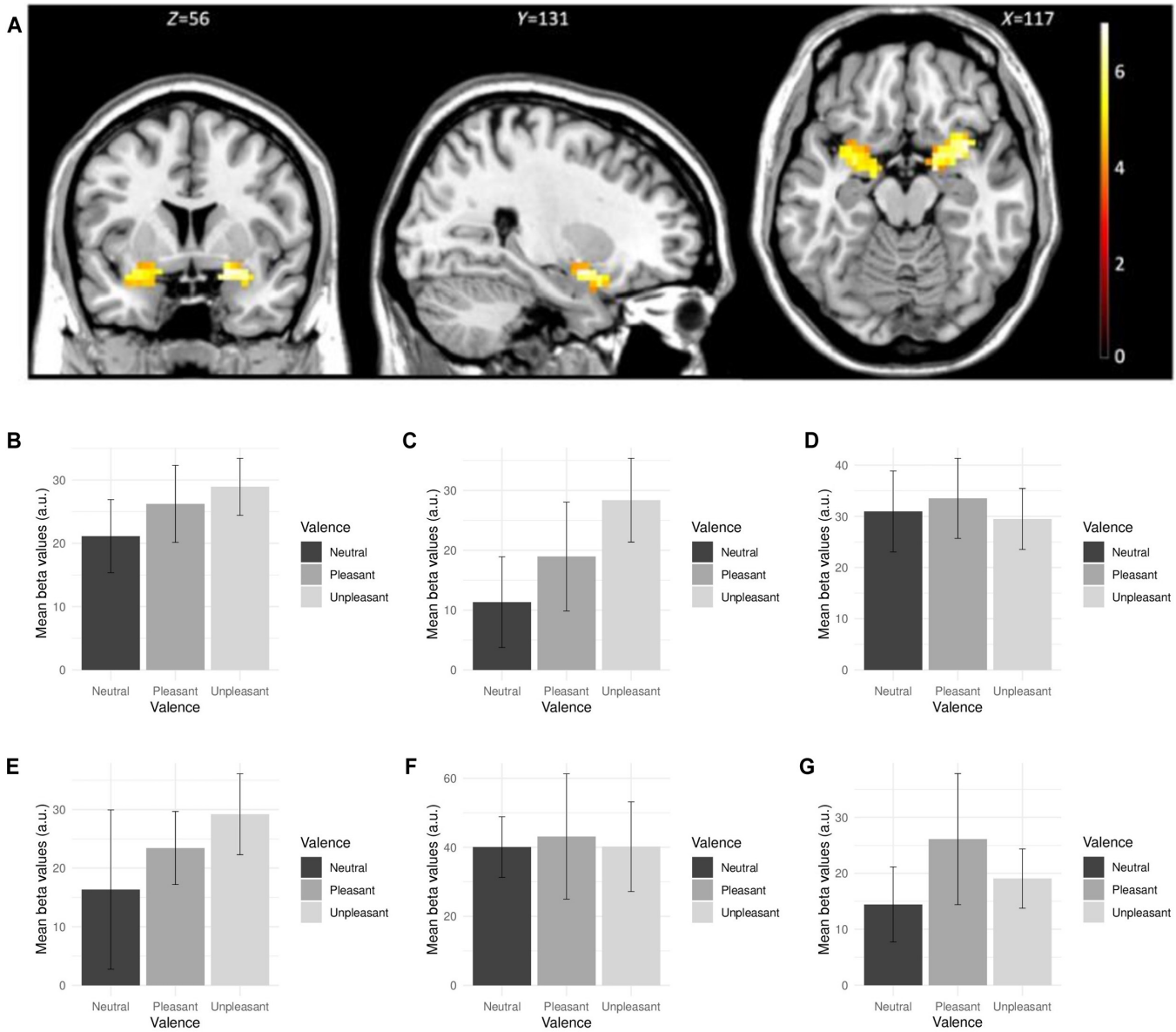

Fig. 4. Functional activations (classical univariate analysis). (A) Group image analysis. (B to D) Mean beta values of neutral, pleasant, and unpleasant odors and their standard errors in AntPC: (B) overall valence effect, (C) effect of valence in left hemisphere, and (D) effect of valence in right hemisphere. (E and F) Mean beta values of neutral, pleasant, and unpleasant odors and their standard errors in PostPC: (E) effect of valence in the left hemisphere and (F) effect of valence in the right hemisphere. (G) Mean beta values of neutral, pleasant, and unpleasant odors and their standard errors in amygdala: overall valence effect.

ordered in an ascending manner according to WRAcc value. For each pattern, the number of voxels involved as well as the participation of the individuals in the pattern, the coordinates of the center of gravity, and the hemisphere involved are mentioned. Finally, Table 3 also integrates the effects of the gender and age factors (*P* values of the statistical tests comparing—for each pattern—the differences between women versus men and young versus old).

One can read in Table 3 that there are 14 patterns (5 unpleasant patterns, 9 pleasant patterns) that have between 3 and 13 voxels. Figures 5 to 10 illustrate these patterns.

Table 3 shows that the participation of the individuals in the pattern is between 42% and 67%. The contribution to the patterns of each individual, as a Shapley value, is also illustrated in the histograms of Figs. 5 to 10 corresponding to the patterns. Furthermore, participation is visualized at the bottom of Figs. 5 to 10 with Venn diagrams (generated using interactivenn [41]). These diagrams make possible the comparison of the participation of individuals in the patterns. Each pattern is represented by a circle or an ellipse and is identified by its classification number according to the WRAcc. The numbers in the overlapping parts between different circles (or ellipses) indicate the number of participants in common between the associated patterns. The number remaining on a single circle (or ellipse) is the number of participants concerning only a specific pattern. The AntPC accounted for 3 patterns, 1 unpleasant (in the left hemisphere, 9 voxels) and 2 pleasant (in the right hemisphere, 5 and 7 voxels), the unpleasant pattern being the one with the highest WRAcc. There are 5 patterns in the posterior piriform cortex (PostPC), 2 unpleasant (in the left hemisphere, 12 and

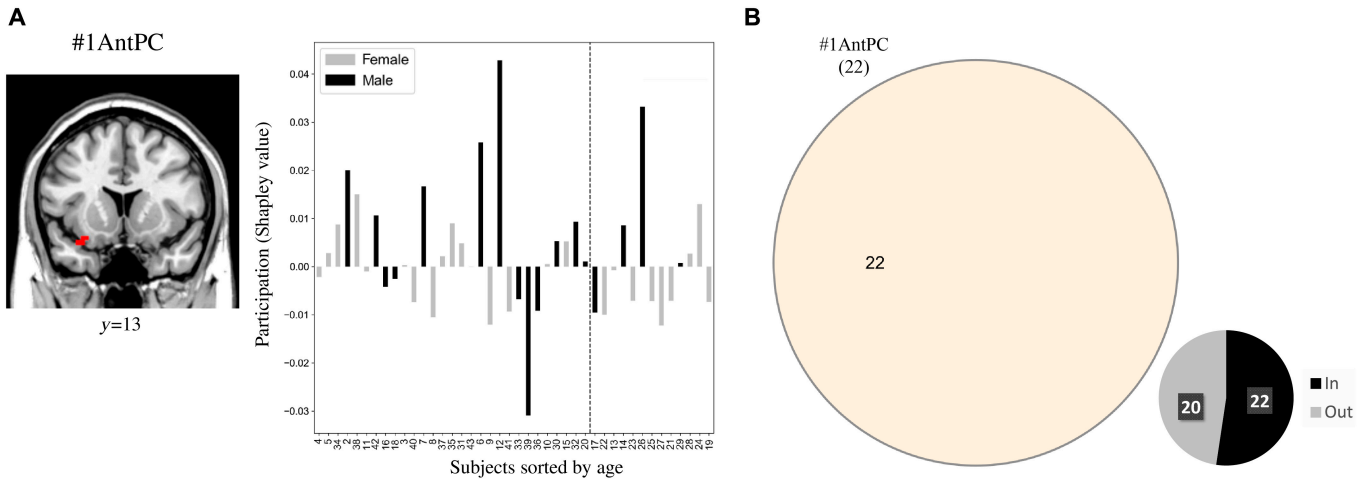

Fig. 5. Unpleasant pattern in the AntPC. (A) A coronal slice shows lateralization. The histogram shows individuals arranged in order of age with "young" individuals to the left of the dashed line and "senior" individuals to the right. Females are in gray and males in black. (B) In this Venn diagram, the pattern is represented by a circle and identified by its classification number according to the WRAcc. The pie chart shows the number of individuals included in the pattern in black and those not included in gray.

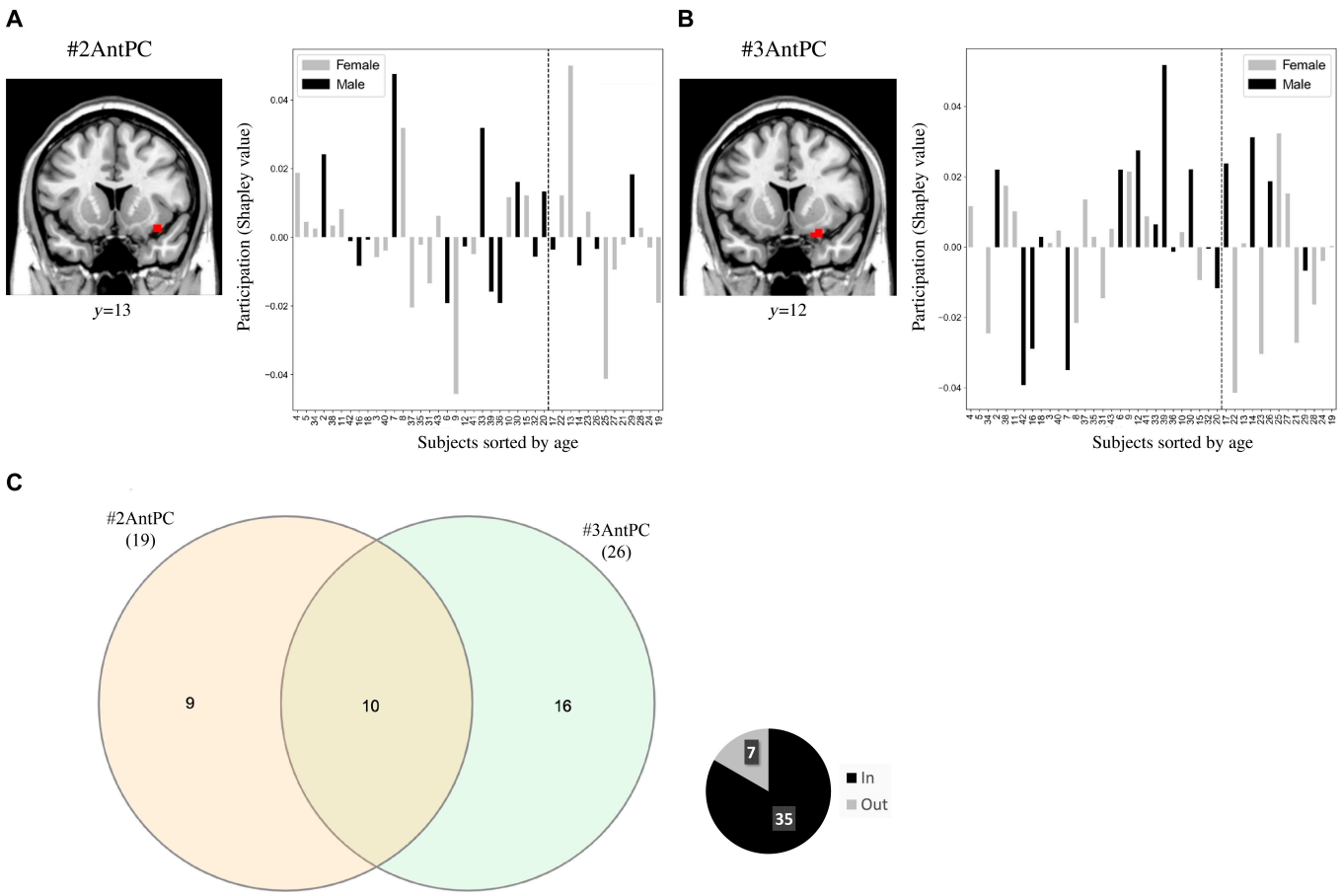

Fig. 6. Pleasant patterns in the AntPC. (A and B) A coronal slice shows the lateralization for each pattern. Each histogram shows individuals arranged in order of age with "young" individuals to the left of the dashed line and "senior" individuals to the right. Females are in gray and males in black. (C) Each pattern is represented by a circle and is identified by its classification number according to the WRAcc. The number in the overlap between the circles indicates the number of participants in common between the 2 patterns. The pie chart shows the number of individuals included in either or both of these patterns in black and those not included in gray.

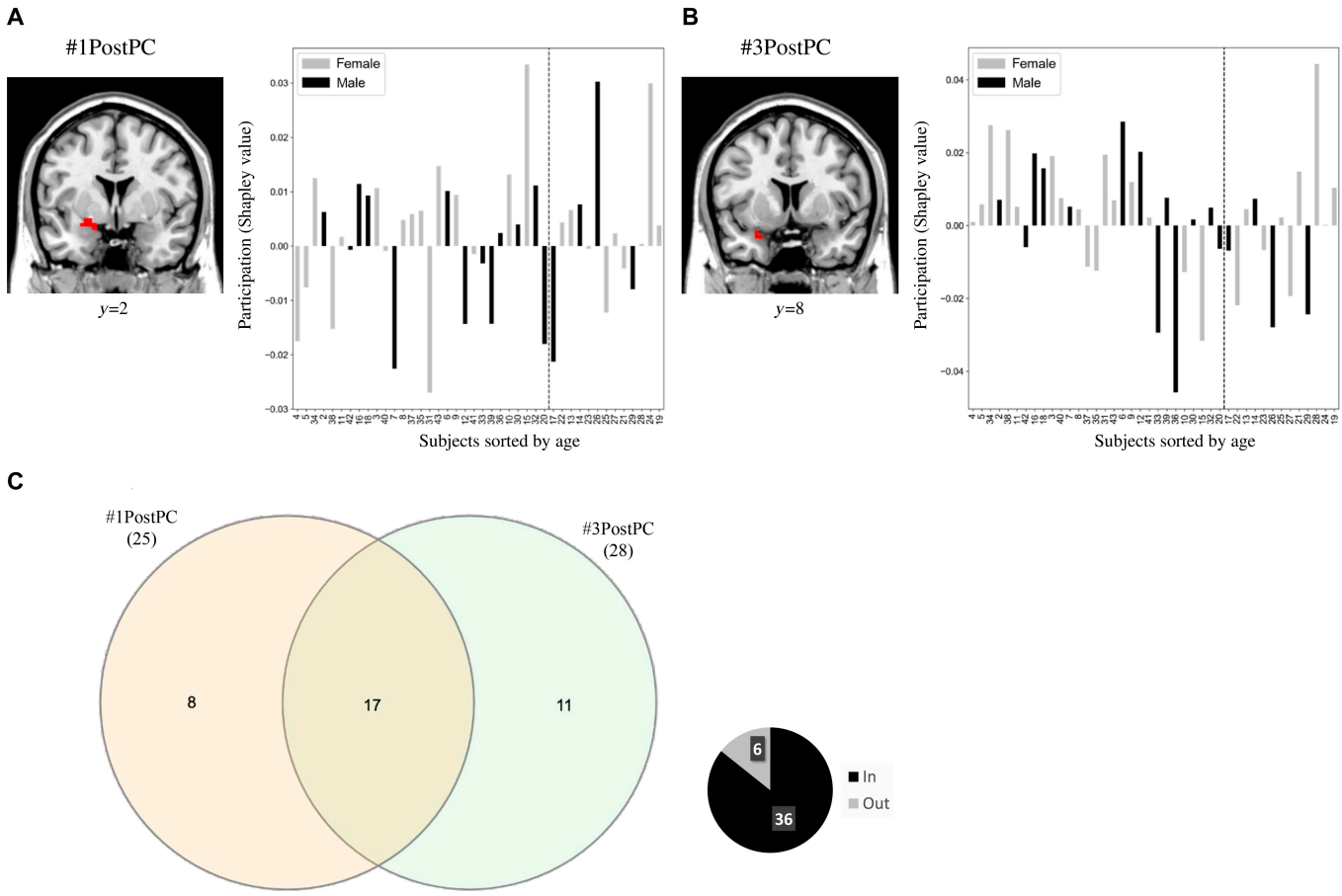

Fig. 7. Unpleasant patterns in the PostPC. (A and B) A coronal slice shows the lateralization for each pattern. Each histogram shows individuals arranged in order of age with "young" individuals to the left of the dashed line and "senior" individuals to the right. Females are in gray and males in black. (C) Each pattern is represented by a circle and is identified by its classification number according to the WRAcc. The number in the overlap between the circles indicates the number of participants in common between the 2 patterns. The pie chart shows the number of individuals included in either or both of these patterns in black and those not included in gray.

6 voxels) and 3 pleasant (one in the left hemisphere, 9 voxels; 2 in the right hemisphere, 4 and 3 voxels), the unpleasant pattern in the left hemisphere being the one with the highest WRAcc. For the amygdala (Amyg), we observe 6 patterns: 2 unpleasant (in the left hemisphere, 13 and 5 voxels) and 4 pleasant (2 in the left hemisphere, 12 and 3 voxels; 2 in the right hemisphere, 8 and 7 voxels). Note that these patterns are not exclusive or totally specific to a condition, as some overlaps between 2 patterns can be observed, as is the case between the #1PostPC pattern and the #1Amyg pattern, and between the #4PostPC pattern and the #4Amyg pattern.

For the study of pattern participation by age and gender, we filtered the itemsets resulting from the discovery of subgroups in order to retain the most relevant and interpretable. In fact, we retain only those results whose informedness is greater than 0.20. In other words, we require at least 20% higher participation of individuals from the target class in the patterns, compared with other classes. As itemsets containing a single item are easier to interpret, only these are shown in Table 4. Young women are more actively involved in pattern #3AntPC, while young men participate more in patterns #4PostPC and #6Amyg. Older women participate more in patterns #4Amyg and #5Amyg, while older men are more involved in pattern #1AntPC. We note that the patterns in which both junior groups participate more frequently correspond to pleasant patterns. Conversely, the older group's exceptional patterns mainly involve unpleasant ones.

Discussion

The spatial localization of pleasant and unpleasant hedonic representations within the piriform/amygdala network is an important question in the field [12,42–46]. Moreover, descriptive analysis methods allowing the quantification and qualification of the contribution of each individual to the observed hedonic pattern in these areas are lacking. Our study is at the heart of these 2 issues.

A univariate analysis classically used in the field revealed that unpleasant odors induced a higher hemodynamic response than neutral or pleasant odors in the anterior portion of the piriform cortex. When this result is combined with (a) psychophysical studies (using reaction times), which show that unpleasant odors are processed more rapidly than pleasant odors [47], and (b) neurophysiological studies, which indicate that olfactomotor activity (sniffing) is less extensive and more rapid in response to an unpleasant odor than a pleasant odor [48,49], it can be hypothesized that the activity in the AntPC reflects early processing of the aversive nature of odors in order to defend the organism against potentially toxic sources. This greater activity for unpleasant odors in the left anterior portion of piriform

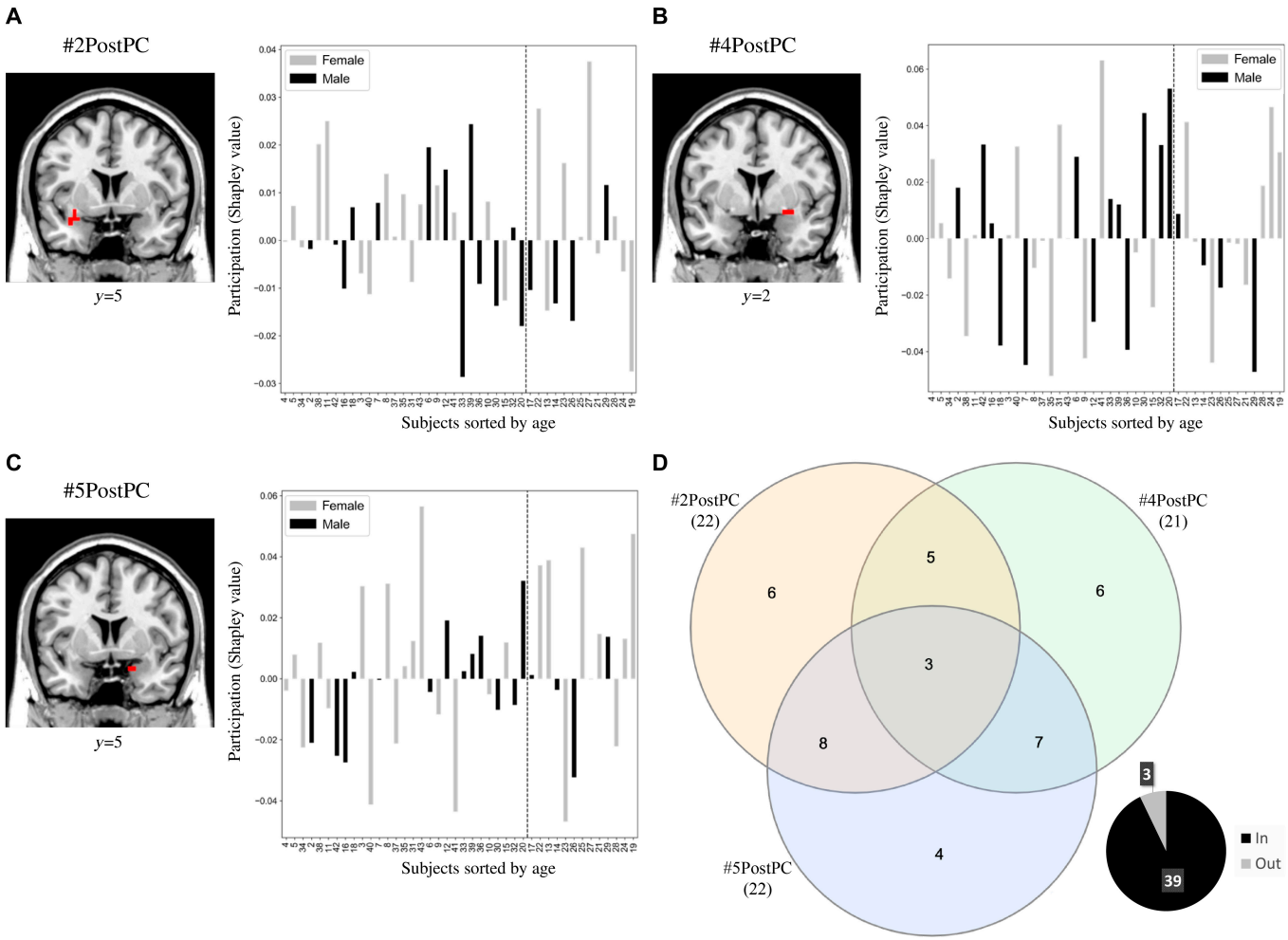

Fig. 8. Pleasant patterns in the PostPC. (A to C) A coronal slice shows the lateralization for each pattern. Each histogram shows individuals arranged in order of age with "young" individuals to the left of the dashed line and "senior" individuals to the right. Females are in gray and males in black. (D) Each pattern is represented by a circle and is identified by its classification number according to the WRAcc. The numbers in the overlapping areas between the circles indicate the number of participants in common between the patterns. The pie chart shows the number of individuals included in one or more of these patterns in black and those not included in gray.

Table 4. Exceptional itemset of size 1 for each class

	Junior			Senior		
	Patterns	Hedonic category	Quality (informedness)	Patterns	Hedonic category	Quality (informedness)
Female	{#3AntPC}	Pleasant	0.212	{#5Amyg} {#4Amyg}	Unpleasant Pleasant	0.465 0.242
Male	{#4PostPC} {#6Amyg}	Pleasant Pleasant	0.279 0.271	{#1AntPC}	Unpleasant	0.25

cortex is in agreement with 2 previous studies [5,17]. The question of lateralization of olfactory processes has given rise to several works. The pioneering work of Zatorre et al. [50] in this area showed a more pronounced involvement of the right hemisphere in olfaction. However, when the hedonic component is taken into account, it seems that the 2 hemispheres make different contributions [8]. Finally, it should be noted that the analysis we performed on other ROIs (PostPC and amygdala) showed no effect of the hedonic valence on the activity of these brain areas. This result is in contradiction with some past studies showing, for example, higher functional activity levels for unpleasant versus pleasant odors in the amygdala [51], although other works suggest that this structure could encode or represent the intensity [11] or salience [15] of the olfactory stimulus rather than its emotional valence.

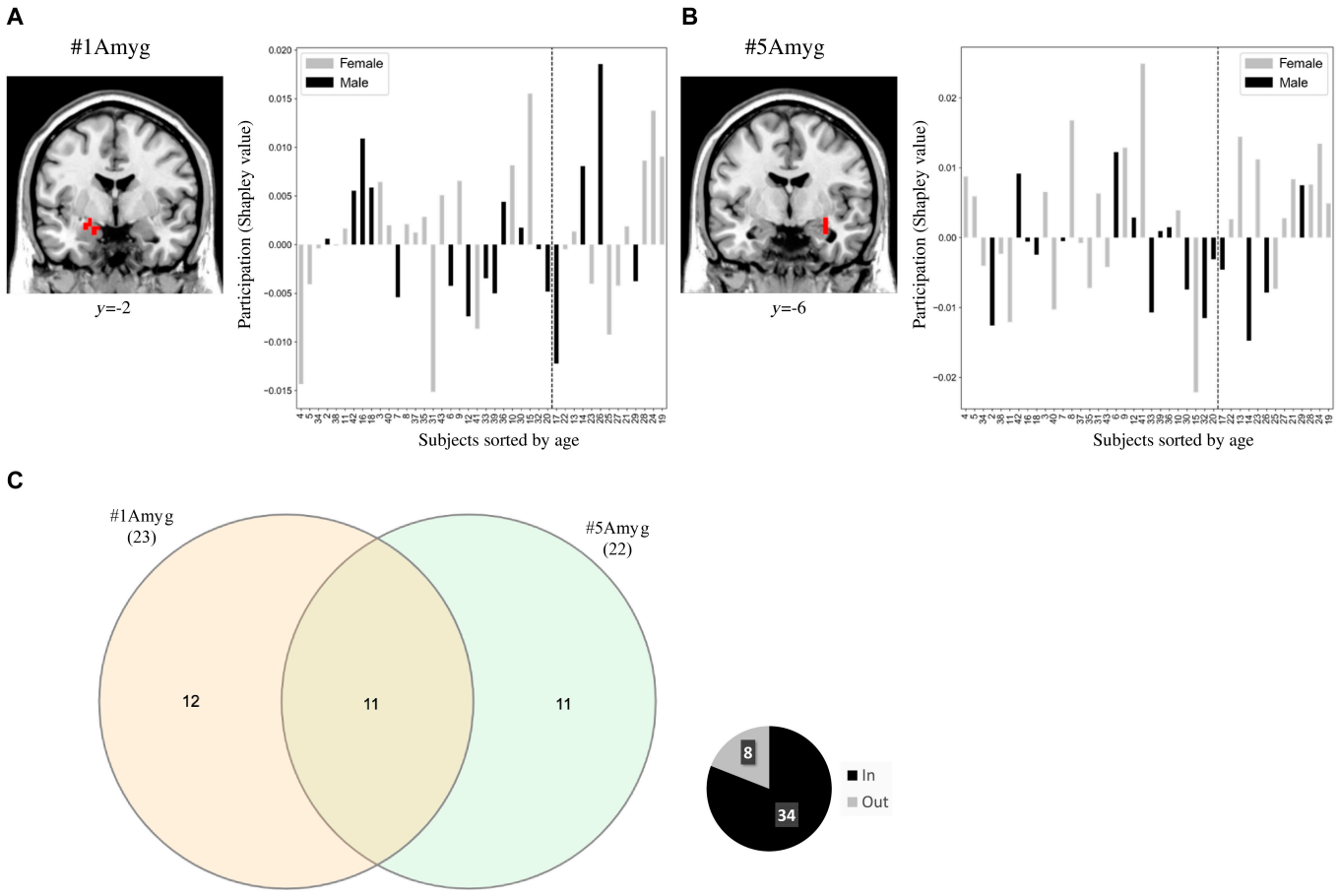

Fig. 9. Unpleasant patterns in the amygdala. (A and B) A coronal slice shows the lateralization for each pattern. Each histogram shows individuals arranged in order of age with "young" individuals to the left of the dashed line and "senior" individuals to the right. Females are in gray and males in black. (C) Each pattern is represented by a circle and is identified by its classification number according to the WRAcc. The number in the overlap between the circles indicates the number of participants in common between the 2 patterns. The pie chart shows the number of individuals included in either or both of these patterns in black and those not included in gray.

The ambition of our approach was to bring additional information to this classical univariate approach via a data mining analysis that allows us to develop descriptive models that take into account the contribution of each tested individual to the observed patterns. This analysis highlighted patterns specific to unpleasant odors on the one hand, and pleasant ones on the other hand. Unlike the univariate analysis, the descriptive analysis revealed patterns related to the hedonic valence in all 3 of the regions studied. In the AntPC, which the univariate analysis found to be significant, the descriptive data mining analysis extracted a spatial localization pattern for unpleasant odors. As in the univariate analysis, this pattern was localized in the left hemisphere. Moreover, in general, the number of patterns generated for pleasant odors was greater than that generated for unpleasant odors, leading to a greater percentage of individuals contributing to unpleasant patterns compared to pleasant patterns. This latter result may illustrate that there is more interindividual agreement in judging an unpleasant odor rather than a pleasant odor. This result is consistent with previous findings using peripheral nervous system activity in response to odors [29]. Finally, we have attempted to compare populations of different sexes and ages. We find that patterns with higher participation from the 2 junior groups related to pleasant odors. Conversely, the majority of patterns within the senior group were associated with unpleasant odors. This observation may be attributed to the shift in odor pleasantness observed as individuals age: Previous research has shown that the hedonic perception of unpleasant odors remains consistent across ages, while odors perceived as pleasant by younger individuals tend to be rated as less pleasant by the elderly [52].

An important question that may be asked in light of the current study concerns the added and applied value of the data mining approach in relation to the classical univariate approaches when dealing with brain functioning. In fact, these 2 approaches complement each other. While the univariate approach allows for the validation of probabilistic and/or predictive models, the data mining approach focuses more on knowledge extraction by providing descriptive and especially explanatory models of the contribution of individuals to the observed patterns. In fact, in our study, because it allows modeling that extracts descriptive rules from the data that link subgroups belonging to both affective and neurobiological spaces, this approach can be positioned at 2 levels compared to univariate analyses: (a) upstream to generate new hypotheses and scientific assumptions that will be testable with, for example, a predictive approach, and (b) at the same time (as in the present paper), to provide complementary information regarding spatial location and the contribution of individuals to the observed patterns.

Moreover, our study enables the development of detailed descriptive models on the role of certain factors of variation

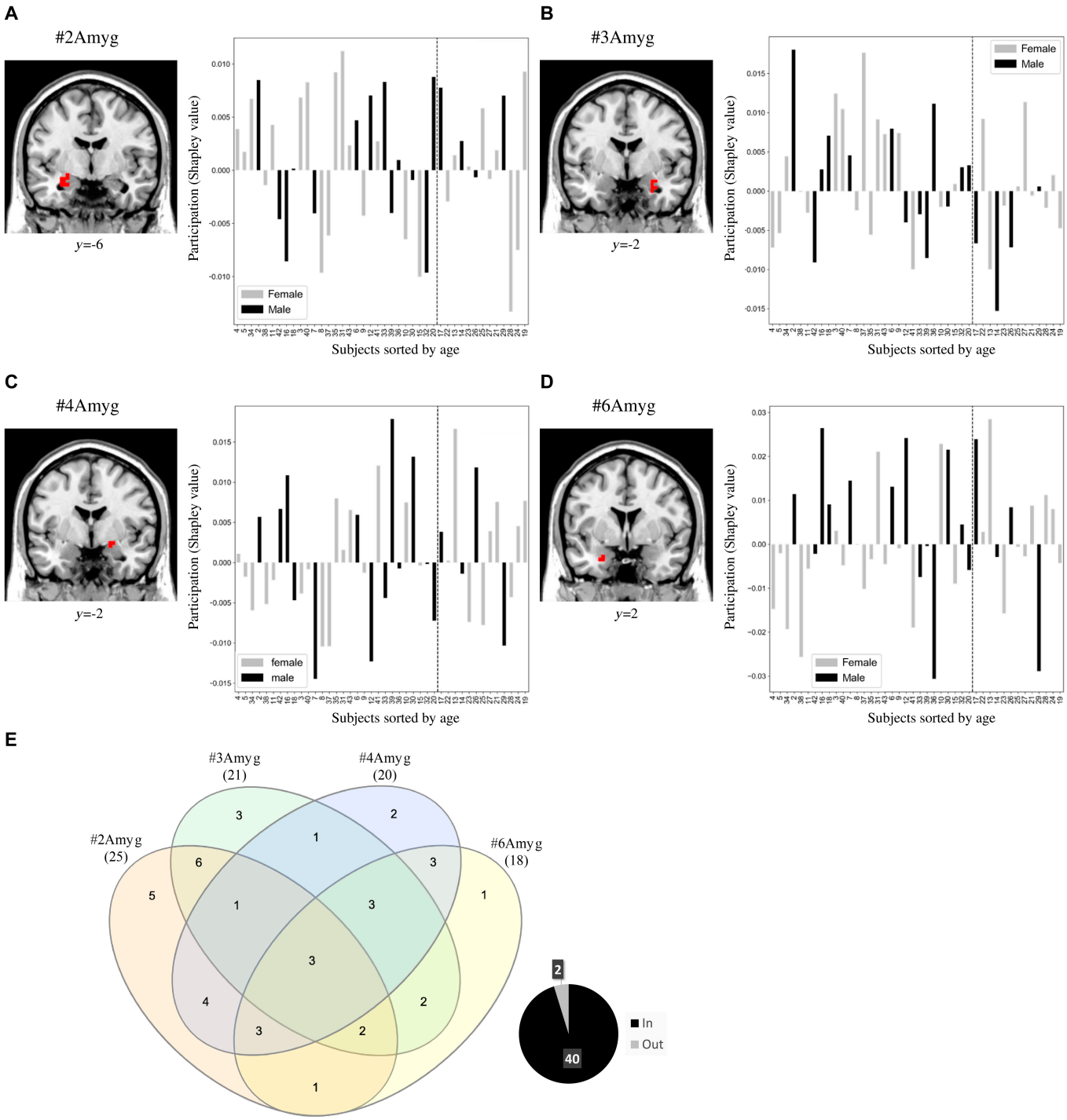

Fig. 10. Pleasant patterns in the amygdala. (A to D) A coronal slice shows the lateralization for each pattern. Each histogram shows individuals arranged in order of age with "young" individuals to the left of the dashed line and "senior" individuals to the right. Females are in gray and males in black. (E) Each pattern is represented by an ellipse and is identified by its classification number according to the WRAcc. The numbers in the overlapping areas between the ellipses indicate the number of participants in common between the patterns. The pie chart shows the number of individuals included in one or more of these patterns in black and those not included in gray.

such as age and sex. In the future, comparisons between pathologies and healthy states could also be considered using such a data mining approach to characterize the influence of specific pathologies on brain activity. Here, data mining could enable a more sophisticated descriptive analysis of the comparisons between individuals (healthy versus pathological), in order to identify the brain regions involved in a given disease, which could pave the way for new curative solutions.

Finally, as a main limitation of the study, it should be noted that the generalizability of our results may be limited by the specific demographic characteristics of the sampled populations. Future research projects could overcome these limitations by employing larger and more diverse cohorts of participants. For example, the

exploration of other factors contributing to olfactory variability in humans, such as genetics, menstrual cycles, satiety, cognition, or even pathologies (as mentioned above), could allow us to delve deeper into the question of affective olfactory diversity.

Conclusion

To sum up, the main objective of the present study was to examine whether the use of exceptional pattern mining can provide new information and thus contribute to improving our understanding of the relationship between odor hedonics and activity in the human amygdala and piriform cortex.

The presented workflow involved data preprocessing, modeling fMRI data in graph form, and extraction of exceptional subgraphs. These extracted patterns underwent analysis to select those deemed relevant and significant. This approach allowed the discovery of specific brain activity associated with the processing of pleasant and unpleasant odors. Subsequently, individual variability was analyzed by exploring the participation of different populations using dedicated algorithms.

Comparisons between the results of this data mining approach and a traditional univariate analysis revealed not only convergences but also the added value of data mining in shedding new light on the contribution of each individual on the observed patterns of neural activity. In particular, our results suggest greater inter-individual variability for pleasant odors than for unpleasant ones, and highlight differences in the processing of hedonic odor perceptions between younger and older individuals. Thus, the inclusion of data mining techniques not only enriches traditional univariate analyses but also offers a unique avenue for generating new hypotheses and elucidating complex relationships between affective and neurobiological spaces.

Acknowledgments

We thank F. Faure, P. Joussain, and C. Sezille from the University of Lyon 1 and D. Ibarrola and her group at the CERMEP brain imaging center.

Funding: This research was funded by the Centre national de la recherche scientifique (CNRS) and the Agence nationale de la recherche (ANR), ChemoSim project.

Author contributions: Conceptualization, methodology, writing—original draft, and writing—review and editing: M.M., A.F., M.P., and M.B. Experimentation tool and software: M.T.

Competing interests: The authors declare that they have no competing interests.

Data Availability

The data are available on request from the corresponding authors.

Supplementary Materials

Figs. S1 to S5
Table S1

References

1. Stevenson RJ. An initial evaluation of the functions of human olfaction. *Chem Senses*. 2010;35(1):3–20.
2. Pinto JM. Olfaction. *Proc Am Thorac Soc*. 2011;8(1):46–52.
3. Lapid H, Shushan S, Plotkin A, Voet H, Roth Y, Hummel T, Schneidman E, Sobel N. Neural activity at the human olfactory epithelium reflects olfactory perception. *Nat Neurosci*. 2011;14(11):1455–1461.
4. Iravani B, Schaefer M, Wilson DA, Arshamian A, Lundström JN. The human olfactory bulb processes odor valence representation and cues motor avoidance behavior. *Proc Natl Acad Sci USA*. 2021;118(42):Article e2101209118.
5. Bensafi M, Sobel N, Khan RM. Hedonic-specific activity in piriform cortex during odor imagery mimics that during odor perception. *J Neurophysiol*. 2007;98(6):3254–3262.
6. Zelano C, Montag J, Johnson B, Khan R, Sobel N. Dissociated representations of irritation and valence in human primary olfactory cortex. *J Neurophysiol*. 2007;97(3):1969–1976.
7. Jin J, Zelano C, Gottfried JA, Mohanty A. Human amygdala represents the complete spectrum of subjective valence. *J Neurosci*. 2015;35(45):15145–15156.
8. Royet JP, Plailly J, Delon-Martin C, Kareken DA, Segebarth C. fMRI of emotional responses to odors: Influence of hedonic valence and judgment, handedness, and gender. *NeuroImage*. 2003;20(2):713–728.
9. Robin O, Alaoui-Ismaïli O, Dittmar A, Vernet-Maury E. Basic emotions evoked by eugenol odor differ according to the dental experience: A neurovegetative analysis. *Chem Senses*. 1999;24(3):327–335.
10. Mantel M, Ferdenzi C, Roy JM, Bensafi M. Individual differences as a key factor to uncover the neural underpinnings of hedonic and social functions of human olfaction: Current findings from PET and fMRI studies and future considerations. *Brain Topogr*. 2019;32(6):977–986.
11. Anderson AK, Christoff K, Stappen I, Panitz D, Ghahremani DG, Glover G, Gabrieli JDE, Sobel N. Dissociated neural representations of intensity and valence in human olfaction. *Nat Neurosci*. 2003;6(2):196–202.
12. Rolls ET, Kringelbach ML, De Araujo IET. Different representations of pleasant and unpleasant odours in the human brain. *Eur J Neurosci*. 2003;18(3):695–703.
13. Fulbright RK, Skudlarski P, Lacadie CM, Warrenburg S, Bowers AA, Gore JC, Wexler BE. Functional MR imaging of regional brain responses to pleasant and unpleasant odors. *Am J Neuroradiol*. 1998;19(9):1721–1726.
14. Gottfried JA, Deichmann R, Winston JS, Dolan RJ. Functional heterogeneity in human olfactory cortex: An event-related functional magnetic resonance imaging study. *J Neurosci*. 2002;22(24):10819–10828.
15. Winston JS, Gottfried JA, Kilner JM, Dolan RJ. Integrated neural representations of odor intensity and affective valence in human amygdala. *J Neurosci*. 2005;25(39):8903–8907.
16. Royet JP, Zald D, Versace R, Costes N, Lavenne F, Koenig O, Gervais R. Emotional responses to pleasant and unpleasant olfactory, visual, and auditory stimuli: A positron emission tomography study. *J Neurosci*. 2000;20(20):7752–7759.
17. Gottfried JA, Dolan RJ. The nose smells what the eye sees: Crossmodal visual facilitation of human olfactory perception. *Neuron*. 2003;39(2):375–386.
18. Howard JD, Plailly J, Grueschow M, Haynes JD, Gottfried JA. Odor quality coding and categorization in human posterior piriform cortex. *Nat Neurosci*. 2009;12(7):932–938.
19. Leman D, Feelders A, Knobbe A. Exceptional model mining. In: *Machine learning and knowledge discovery in databases*. European Conference, ECML PKDD. Berlin Heidelberg: Springer; 2008. p. 1–16.

20. Bendimerad A, Plantevit M, Robardet C. Mining exceptional closed patterns in attributed graphs. *Knowl Inf Syst*. 2018;56(1):1–25.
21. Pouliot S, Bourgeat F, Barkat S, Rouby C, Bensafi M. Increase in anhedonia level in menopausal women is accompanied by a shift in olfactory function. *Chemosens Percept*. 2008;1(1):43–47.
22. Doty R, Kamath V. The influences of age on olfaction: A review. *Front Psychol*. 2014;5:20.
23. Sorokowski P, Karwowski M, Misiak M, Marczak MK, Dziekan M, Hummel T, Sorokowska A. Sex differences in human olfaction: A meta-analysis. *Front Psychol*. 2019;10:242.
24. Fournel A, Ferdenzi C, Sezille C, Rouby C, Bensafi M. Multidimensional representation of odors in the human olfactory cortex. *Hum Brain Mapp*. 2016;37(6):2161–2172.
25. Joussain P, Bessy M, Faure F, Bellil D, Landis BN, Hugentobler M, Tuorila H, Mustonen S, Vento SI, Delphin-Combe F, et al. Application of the European Test of Olfactory Capabilities in patients with olfactory impairment. *Eur Arch Otorrinolaringol*. 2016;273(2):381–390.
26. Thomas-Danguin T, Rouby C, Sicard G, Vigouroux M , Farget V, Johanson A, Bengtzon A, Hall G, Ormel W, De Graaf C, et al. Development of the ETOC: A European test of olfactory capabilities. *Rhinology*. 2003;41:142–151.
27. Sezille C, Messaoudi B, Bertrand A, Joussain P, Thévenet M, Bensafi M. A portable experimental apparatus for human olfactory fMRI experiments. *J Neurosci Methods*. 2013;218(1):29–38.
28. Macqueen J. Some methods for classification and analysis of multivariate observations. *Proc. Fifth Berkeley Symp. Math. Stat. Prob.* 1967;1(14):281–297.
29. Moranges M, Plantevit M, Bensafi M. Using subgroup discovery to relate odor pleasantness and intensity to peripheral nervous system reactions. *IEEE Trans Affect Comput*. 2022.
30. Esteban O, Markiewicz CJ, Blair RW, Moodie CA, Isik AI, Erramuzpe A, Kent JD, Goncalves M, DuPre E, Snyder M, et al. fMRIPrep: A robust preprocessing pipeline for functional MRI. *Nat Methods*. 2019;16(1):111–116.
31. Behzadi Y, Restom K, Liau J, Liu TT. A component based noise correction method (CompCor) for BOLD and perfusion based fMRI. *NeuroImage*. 2007;37(1):90–101.
32. Ashburner J, Barnes G, Chen CC, Daunizeau J, Flandin G, Friston KJ, Gitelman D, Glauche V. Henson R, Hutton C, et al. *SPM12 Manual—The FIL Methods Group (and Honorary Members)*. London (UK): Functional Imaging Laboratory, Wellcome Centre for Human Neuroimaging, UCL Queen Square Institute of Neurology; 2021.
33. Tzourio-Mazoyer N, Landeau B, Papathanassiou D, Crivello F, Etard O, Delcroix N, Mazoyer B, Joliot M. Automated anatomical labeling of activations in SPM using a macroscopic anatomical parcellation of the MNI MRI single-subject brain. *NeuroImage*. 2002;15(1):273–289.
34. Rolls ET, Joliot M, Tzourio-Mazoyer N. Implementation of a new parcellation of the orbitofrontal cortex in the automated anatomical labeling atlas. *NeuroImage*. 2015;122:1–5.
35. Rolls ET, Huang CC, Lin CP, Feng J, Joliot M. Automated anatomical labelling atlas 3. *NeuroImage*. 2020;206:Article 116189.
36. Midroit M, Chalençon L, Renier N, Milton A, Thevenet M, Sacquet J, Breton M, Forest J, Noury N, Richard M, et al. Neural processing of the reward value of pleasant odorants. *Curr Biol*. 2021;31(8):1592–1605.e9.
37. Lavrac N, Kavsek B, Flach P, Todorovski L. Subgroup discovery with CN2-SD. *J Mach Learn Res*. 5(2):153–188.
38. Kuhn HW, Tucker AW. *Contributions to the theory of games*. Princeton (NJ): Princeton University Press; 1953.
39. Castro J, Gómez D, Tejada J. Polynomial calculation of the Shapley value based on sampling. *Comput Oper Res*. 2009;36(5):1726–1730.
40. Mathonat R, Nurbakova D, Boulicaut JF, Kaytoue M. Anytime mining of sequential discriminative patterns in labeled sequences. *Knowl Inf Syst*. 2021;63(2):439–476.
41. Heberle H, Meirelles GV, da Silva FR, Telles GP, Minghim R. InteractiVenn: A web-based tool for the analysis of sets through Venn diagrams. *BMC Bioinformatics*. 2015;16(1):169.
42. Djordjevic J, Boyle JA, Jones-Gotman M. Pleasant or unpleasant: Attentional modulation of odor perception. *Chemosens Percept*. 2012;5(1):11–21.
43. Paradiso S, Johnson DL, Andreasen NC, O'Leary DS, Watkins GL, Boles Ponto LL, Hichwa RD. Cerebral blood flow changes associated with attribution of emotional valence to pleasant, unpleasant, and neutral visual stimuli in a PET study of normal subjects. *Am J Psychiatry*. 1999;156(10):1618–1629.
44. Masaoka Y, Koiwa N, Homma I. Inspiratory phase-locked alpha oscillation in human olfaction: Source generators estimated by a dipole tracing method. *J Physiol*. 2005;566(3):979–997.
45. Grabenhorst F, Rolls ET, Margot C, MAAP S, Velazco MI. How pleasant and unpleasant stimuli combine in different brain regions: Odor mixtures. *J Neurosci*. 2007;27(49):13532–13540.
46. Herbert C, Ethofer T, Anders S, Junghofer M, Wildgruber D, Grodd W, Kissler J. Amygdala activation during reading of emotional adjectives—An advantage for pleasant content. *Soc Cogn Affect Neurosci*. 2009;4(1):35–49.
47. Bensafi M, Rouby C, Farget V, Bertrand B, Vigouroux M, Holley A. Perceptual, affective, and cognitive judgments of odors: Pleasantness and handedness effects. *Brain Cogn*. 2003;51(3):270–275.
48. Johnson BN, Mainland JD, Sobel N. Rapid olfactory processing implicates subcortical control of an olfactomotor system. *J Neurophysiol*. 2003;90(2):1084–1094.
49. Bensafi M, Porter J, Pouliot S, Mainland J, Johnson B, Zelano C, Young N, Bremner E, Aframian D, Khan R, et al. Olfactomotor activity during imagery mimics that during perception. *Nat Neurosci*. 2003;6(11):1142–1144.
50. Zatorre RJ, Jones-Gotman M, Evans AC, Meyer E. Functional localization and lateralization of human olfactory cortex. *Nature*. 1992;360(6402):339–340.
51. Zald DH, Pardo JV. Emotion, olfaction, and the human amygdala: Amygdala activation during aversive olfactory stimulation. *Proc Natl Acad Sci USA*. 1997;94(8):4119–4124.
52. Joussain P, Thevenet M, Rouby C, Bensafi M. Effect of aging on hedonic appreciation of pleasant and unpleasant odors. *PLOS ONE*. 2013;8(4):Article e61376.